A Continuum-Atomistic Multi-Timescale Algorithm for Micro/Nano Flows[†]

Jin Liu[1,*], Shiyi Chen[1,2], Xiaobo Nie[3,4] and Mark O. Robbins[1,3]

[1] *Department of Mechanical Engineering, Johns Hopkins University, Baltimore, MD 21218, USA.*
[2] *State Key Laboratory for Turbulence and Complex Systems, College of Engineering and Center for Computational Science and Engineering, Peking University, Beijing, China.*
[3] *Department of Physics and Astronomy, Johns Hopkins University, Baltimore, MD 21218, USA.*
[4] *Exa Corporation, Burlington, MA 01803, USA.*

Abstract. A multi-timescale algorithm is proposed for simulating time-dependent problems in micro- and nano- fluidics. The total simulation domain is spatially decomposed into two regions. Molecular dynamics is employed in the crucial interfacial regions and continuum hydrodynamics is adopted in the remaining bulk regions. The coupling is through "constrained dynamics" in an overlap region. Our time scheme is based on the time scale separation between the continuum macro time step and molecular micro time step. This allows the molecular dynamics during one macro time step to be treated as in quasi-steady state. Therefore, molecular simulation is only performed in two shorter time intervals. Through linear extrapolation of macroscopic velocities and re-initialization of particle configurations, we can significantly reduce the total computational cost. We demonstrate and discuss our time algorithm through hybrid simulation of channel flow driven by a sinusoidally moving top wall. Converging results are achieved for cases of large separation of time scale with much less computational cost than with the original hybrid simulation without time extrapolation.

1 Introduction

Continuum hydrodynamics with simple constitutive relations and no-slip boundary conditions is quite successful in describing macroscopic fluid flows, but may fail in many situations in micro and nano engineering where molecular detail is important. In principle, classical molecular dynamics (MD) can provide all the detailed information and is capable of resolving all the problems. However, performing a MD simulation on the required spatial and temporal scales is computationally impractical due to the extremely tiny spatial and temporal scales associated with molecular motion. It has been observed that in many common scenarios, molecular details are required only in small spatial regions such as solid-fluid or fluid-fluid interfaces, while the continuum descriptions are still accurate in the remaining bulk regions. Therefore, it is desirable to develop a hybrid method to combine the efficiency of continuum hydrodynamics and accuracy of MD simulation.

Several hybrid schemes have been developed for simulating dense liquid systems in the last decade. Most are based on "domain decomposition", in which the simulation domain is decomposed into two regions. MD is adopted in small crucial regions where molecular details are important and continuum hydrodynamics is used in the remaining bulk regions. A coupling algorithm must be developed to ensure the consistency of these two completely different descriptions, and this is the heart of all hybrid methods.

O'Connell and Thompson [1] suggested coupling via a finite overlap region to avoid sharp transitions and used a relaxation method to ensure consistency of velocities between MD and continuum regions. They successfully implemented their approach in simulating simple one dimensional Couette flow. Hadjiconstantinou and Patera [2] introduced a Maxwell Demon method and they employed a momentum reservoir to constrain the particle velocities. The Schwarz iteration method was adopted to ensure MD and continuum descriptions were consistent. Examples of steady state channel flow with obstacles [2] and moving contact-line problems [3] were used to demonstrated their method. Flekkoy *et al.* [4] proposed a coupling scheme based on the continuity of mass and momentum fluxes for simulating compressible flows. In their recent works [5,6], they also accounted for the energy flux in their examples. Buscalioni and Coveney [7,8] also adopted the flux coupling scheme and demonstrated their approach by simulation of transversal and longitudinal waves.

More recently, Nie *et al.* [9] developed a coupling scheme using Lagrange multipliers for simulating isothermal, incompressible flows. In their approach, the particle velocities were constrained in the overlap region such that the average particle velocities were equivalent to the instantaneous continuum velocities. They have successfully implemented their approach for simulating driven cavity flow [10,11] and moving contact-line problems. Most recently Liu *et al.* [12] extended the scheme developed in [9] to incorporate thermal effects. Based on Nie *et al.* 's work [9], several minor modifications of the constrained equations have also been proposed. Wang and He [13] proposed a dynamic coupling model in which the coupling parameter in the constrained equations

was determined dynamically at each time step based on the current state. Yen *et al.* [14] suggested that a time-averaged value should be adopted in evaluation of the constrained force to reduce the statistical fluctuations and improve the convergence rate. However, since the time scales of atomistic and continuum simulations are still coupled in their schemes, the separation of time scales limited the application of their methods to either dynamic problems with a short time period or steady state problems.

Ren and E [15] proposed a very different hybrid scheme. Instead of decomposing the simulation domain into MD and continuum parts, they employed the continuum solver in the entire domain. Missing information, such as the momentum fluxes and boundary conditions was extracted from local MD simulations. While they claimed this approach decoupled the time scales, they only demonstrated their approach on steady state problems. A detailed discussion and comparison of their scheme with other hybrid schemes can be found in a recent review article [16].

Here we propose a time scheme to further accelerate the hybrid scheme developed in [9] that is similar in concept to the "equation free" approach proposed by Kevrekidis *et al.* [17]. The scheme is based on the fact that the macro time step associated with continuum calculations is generally orders of magnitude larger than the micro time step associated with molecular dynamics. We thus assume that the evolution of molecular dynamics can be treated as quasi-steady state. Therefore, instead of performing the MD simulation in the entire macro time step, we merely conduct the MD in two successive shorter time periods. Through linear extrapolation of macroscopic variables and re-initialization of the molecular dynamics, the total computational cost of the hybrid simulations can be significantly reduced while atomistic details are still retained.

In this contribution, we first briefly outline the "domain decomposition" and "constrained dynamics", and then focus on the proposed time scheme in Section 2. In Section 3, we demonstrate our hybrid scheme through simulation of channel flow driven by oscillatory wall motion. The conclusions and discussions are presented in the last section.

2 Numerical algorithm

2.1 Domain decomposition and coupling scheme

Fig. 1 is the schematic of the "domain decomposition" applied in our calculations. As illustrated, the total computational domain is spatially divided into two parts: the particle part indicated by dots and the continuum part represented by shading. MD simulations are performed in the particle domain and continuum fluid dynamics equations are solved in the continuum domain. Both descriptions are integrated in an overlap region, which typically extends several continuum grid sizes between particle and continuum domains. This overlap region plays a key role in our hybrid scheme. As described in the following, consistency between MD and continuum domains is ensured through communication between these two domains in the overlap region.

As displayed in Fig. 1, the particle domain contains two layers of solid wall molecules
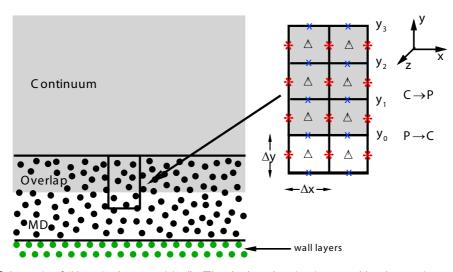
Figure 1: Schematic of "domain decomposition". The shadowed region is treated by the continuum description and the dotted region is treated by the atomistic description. In the enlarged overlap region (right), at $P \to C$ coarse-grained MD solutions provide boundary conditions for continuum simulations, and in $C \to P$ molecular motion is constrained according to continuum solutions in the corresponding region. A staggered grid is employed in continuum simulations, in which p is defined at cell centers (triangles) and velocity components at the middle of the perpendicular cell edges (crosses and asterisks).

and an ensemble of fluid molecules above it. The arrangement of the solid molecules follows the fcc (111) crystal lattice, and they are kept stationary at their equilibrium positions during the simulations. Fluid molecules are distributed above the solid wall and the interaction forces between fluid molecules are modeled with the truncated and shifted Lennard-Jones potential,

$$V^{LJ}(r) = 4\epsilon \left[\left(\frac{\sigma}{r} \right)^{12} - \left(\frac{\sigma}{r} \right)^{6} - \left(\frac{\sigma}{r_c} \right)^{12} + \left(\frac{\sigma}{r_c} \right)^{6} \right], \tag{2.1}$$

where ϵ is the characteristic binding energy and σ is the characteristic length, representing the fluid molecule diameter. To reduce the computational cost, the interaction forces are set to zero when the distance between molecules is more than a cutoff length $r_c = 2.2\sigma$. We set the fluid density $\rho = 0.81 m\sigma^{-3}$ to be consistent with previous simulations [9–12], where m is the particle mass. The interaction forces between solid and fluid molecules are also modeled with a shifted Lennard-Jones potential (2.1) with the characteristic binding energy $\epsilon^{wf} = 0.6\epsilon$ and characteristic length $\sigma^{wf} = \sigma$. This selection of parameters leads to a no-slip boundary condition at the fluid-solid interface.

The motion of fluid particles follows Newton's laws. The equations of motion are integrated using the velocity-Verlet scheme with a time step of $\Delta t_{MD} = 0.005\tau$, where $\tau = (m\sigma^2/\epsilon)^{1/2}$ is the characteristic time of the Lennard-Jones potential. Periodic boundary conditions are applied in both x and z directions. We maintain the system at constant temperature T, although our time scheme could readily be extended to studies of thermal

transport. A Langevin thermostat [18] with damping rate τ^{-1} is applied in the flow-irrelevant z direction. As in previous studies [9–11], $T = 1.1\epsilon/k_B$ where k_B is Boltzmann's constant. At this T, the fluid's dynamic viscosity is $\mu = 2.14\epsilon\tau\sigma^{-3}$ [1] and this value is applied in the following continuum equations.

In the continuum domain, the dynamics are effectively two-dimensional (2D) because there is no variation along z. The following 2D incompressible Navier-Stokes equations are solved

$$\begin{cases} \nabla\cdot\mathbf{u}=0, \\ \partial_t\mathbf{u}+\mathbf{u}\cdot\nabla\mathbf{u}=-\frac{1}{\rho}\nabla p+\nu\nabla^2\mathbf{u}, \end{cases} \tag{2.2}$$

where $\mathbf{u}$ is the fluid velocity, p corresponds to pressure and $\nu = \mu/\rho = 2.64\epsilon\tau/m$ is the kinematic viscosity of the fluid. The N-S equations are solved on a staggered grid [19] in which pressure is defined at the center of the grid and velocities in the middle of the sides of the grid as indicated in Fig. 1. A no-slip boundary condition is imposed at the top wall and periodic boundary conditions are applied along the x (streamwise) direction.

The key issue for any hybrid scheme lies in the coupling of atomistic and continuum descriptions in the overlap region. The molecular dynamics and continuum hydrodynamics mutually provide boundary conditions to each other. As indicated in Fig. 1, at the lower edge of the continuum domain, $y = y_0$, the coarse-grained MD values of y direction velocities at crosses along $y = y_0$ and x direction velocities at asterisks along $y = y_0 - \Delta y/2$ are fed into the continuum calculation as boundary conditions. The coarse-graining process includes averaging spatially over the volume of a grid cell $\Delta x \times \Delta y \times \Delta z$ that is centered on the point of interest and temporally over time intervals as described in Sec. 2.2. In addition, to reduce noise and make use of parallel processors, an ensemble of $N_{ensemble}$ realizations of the MD region is simulated and the results averaged.

In the region between y_1 and y_2, the continuum solutions in each grid cell serve as boundary conditions for MD simulation. This is achieved through so-called "constrained dynamics". Suppose $\mathbf{u}_J$ is the average continuum velocity in cell J. Then continuity of the mean velocity requires that the coarse-grained particle velocity in this cell is equal to $\mathbf{u}_J$. As shown in [9], finding the extremum of the time integral of the Lagrangian for particles subject to this nonholonomic constraint leads to modified equations of motion for the i-th particle in cell J:

$$\ddot{\mathbf{x}}_i = \frac{\mathbf{F}_i}{m} - \frac{1}{N_J m}\sum_{k=1}^{N_J}\mathbf{F}_k + \frac{D\mathbf{u}_J(t)}{Dt}, \tag{2.3}$$

where $\mathbf{F}_i$ is the sum of Lennard-Jones forces (2.1) from other particles, $\mathbf{F}_i = -\frac{\partial}{\partial x_i}\sum_{j\neq i}V^{LJ}(r_{ij})$, N_J is the number of particles in cell J, and D/Dt denotes the material derivative. The two extra terms at the end of (2.3) ensure that the mean particle velocity follows the continuum solution.

To prevent particles from leaving the domain, an external nonlinear force is applied

in the region between y_2 and y_3:

$$F_y = -\alpha p_0 \sigma \frac{(y-y_2)}{1-(y-y_2)/(y_3-y_2)}. \tag{2.4}$$

Here $p_0 = 3.16\epsilon/\sigma^3$ is the equilibrium pressure of the fluid and α is a constant of order one. As discussed in [12], this nonlinear force in the region above y_2 ensures that the particle density is constant over the constraining region ($y_1 < y < y_2$). Then the density decays smoothly and rapidly to zero over about 1σ above y_2. Another effect of this buffer region $y > y_2$ is to help equilibrate particles that are added to the system as explained in the following.

To account for mass flux, the particle flux across the MD-continuum interface $y = y_2$ is calculated from the continuum velocity field. The change in the number of particles in a cell during Δt_{FD} is

$$\Delta n = -A\rho u_y \Delta t_{FD}/m, \tag{2.5}$$

where A is the area of the cell perpendicular to the interface. The change in number is integrated until its magnitude exceeds an integer n'. If n' is negative, the n' atoms closest to y_3 are removed. If n' is positive, n' atoms are inserted at evenly spaced time intervals over the relaxation period described in Sec. 2.2. The fractional remainder is added to the flux at the next time interval. Particles are added at random positions in the $x-z$ plane and 1σ above the particle in the cell that has the largest y. The initial velocity of an inserted particle is equal to the continuum velocity in the corresponding cell, and the peculiar velocities in the buffer region are coupled to a Langevin thermostat which has the same temperature as the remaining MD region.

2.2 Time algorithm

The time scheme implemented in our simulations is illustrated in Fig. 2. The extension of our method to heat transfer problems is straightforward, therefore, we will only focus our discussion on isothermal systems. The spatial decomposition is indicated on the x axis and the temporal decomposition is illustrated on the t axis. As shown, $\Delta t_{MD} = 0.005\tau$ represents the time step used in MD calculations which is associated with microscopic molecular motions. Δt_{FD} is the time step adopted in the continuum calculation which is associated with macroscopic flow. For small Reynolds number flows, the continuum time step Δt_{FD} must be smaller than the characteristic time of flows on the grid scale $\rho \Delta x \Delta y/\mu$. The basic motivation of the time algorithm is based on the fact that there is a large time separation between continuum time step Δt_{FD} and MD time step Δt_{MD}. Due to the time separation and large number of molecular particles contained in the particle region, the dominant computational cost of previous methods is in the MD domain even though this region may be very small spatially compared with the remaining continuum region.
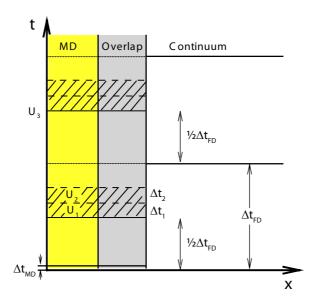
Figure 2: Schematic of the time scheme implemented in this paper. The x axis indicates the spatial decomposition and the t axis indicates temporal separation. Δt_{FD} is the continuum time step and Δt_{MD} is the molecular simulation time step. The MD is performed in time intervals of Δt_1 and Δt_2 starting at the midpoint between continuum time steps. U_1 and U_2 are the respective coarse-grained velocities. They are used to linearly extrapolate coarse-grained velocities to values U_3 at the start of the next MD interval (2.6). MD is performed over a short relaxation period Δt_r to produce an initial microscopic state consistent with the U_3.

The fact that the variation of macroscopic velocities associated with molecular dynamics must be small during one continuum time step allows us to treat the molecular dynamics as quasi-steady state. Then, in the MD domain the macroscopic velocities evolve linearly with time during the continuum time step Δt_{FD}. Therefore, as shown in Fig. 2, during one iteration of the hybrid calculation in the particle domain (including the overlap region), instead of performing MD simulation in the entire time Δt_{FD}, we conduct molecular simulation in two shorter successive time intervals Δt_1 and Δt_2. The first starts at the midpoint between continuum time steps and uses velocity boundary conditions obtained by extrapolating the continuum solution from the two previous macro time steps. Coarse-grained velocities U_1 and U_2 for each grid cell are obtained from the MD simulation by averaging spatially over the cell and temporally over Δt_1 and Δt_2, respectively. Then U_i represents the macroscopic velocity at a time in the center of the corresponding averaging interval. The goal is to use these velocities to obtain appropriate states for MD simulations at the midpoint of the next continuum time interval. Coarse-grained velocities U_3 for each cell at this later time are obtained by a linear extrapolation:

$$U_3 = U_2 + (U_2 - U_1)\frac{\Delta t_{FD} - \Delta t_1 - \Delta t_2/2}{\Delta t_1/2 + \Delta t_2/2}. \tag{2.6}$$

The FD equations are then integrated one step and extrapolated to obtain new continuum boundary conditions for the MD simulations.

The above steps specify the coarse-grained state of the system at the time corresponding to U_3. The final step of the algorithm is creation of microscopic particle configurations and velocities that are consistent with U_3 and can be used as initial conditions for the next MD simulation interval. We call this the re-initialization process. The simplest approach would be to take the final state from Δt_2 and shift the velocity of each atom by the change in coarse-grained velocity in its cell. This produces discontinuities in local velocity at cell boundaries and led to numerical instabilities. Instead, we used a relaxation process that is equivalent to accelerating the time. The MD equations were integrated over a relaxation time Δt_r during which the mean velocities in all cells were constrained to change linearly to U_3 from their values at the end of Δt_2. The constraint dynamics were the same as in the previous section, with the material derivative in Eq. (2.3) calculated as $(U_3-U_2)/\Delta t_r$. The value of Δt_r must be chosen to be much larger than the velocity autocorrelation time and the time for sound propagation across the cell in order to be sure that transients have relaxed. As noted above, particles are added or subtracted to match the continuum flux at the outer boundary of the overlap region during the re-initialization process. Because we consider incompressible flows, changes in the number of particles in other cells can be neglected.

3   Results and discussions

Finite spatial and temporal averages of particle velocities necessarily include thermal noise. For instance, the averaged velocity U_1 in a cell can be written as $U_1 = \bar{U}_1 + \Delta U_1$ in which $\bar{U}_1$ is the desired signal while ΔU_1 is the thermal noise. During the linear extrapolation in Eq. (2.6) the thermal noise is also exaggerated. The ratio between noise and signal in the velocity change between MD intervals is defined as

$$\frac{\left[\langle(\Delta U_2-\Delta U_1)^2\rangle\right]^{0.5}}{\bar{U}_2-\bar{U}_1} = \frac{\sqrt{2}\Delta U(\Delta t_{AV})}{\bar{U}_2-\bar{U}_1}, \tag{3.1}$$

where angular brackets indicate a statistical average, $\Delta t_{AV} = \Delta t_1 = \Delta t_2$ is the averaging time, ΔU_1 and ΔU_2 are assumed to add incoherently, and ΔU is the rms error in each interval. The thermal noise

$$\Delta U(\Delta t_{AV}) = \frac{u_T}{\sqrt{N_{cell}N_{ensemble}}\sqrt{\Delta t_{AV}/t_{vv}}}, \tag{3.2}$$

where $u_T = \sqrt{mk_BT}$ is the rms variation in each component of the velocity associated with the fluid temperature, N_{cell} is the number of atoms in each grid cell, $N_{ensemble}$ is the number of independent ensembles in our calculation and t_{vv} is the velocity auto-correlation time. For our situation $t_{vv} \sim 0.14\tau$ [1]. The absolute error in the extrapolated velocity is increased by the ratio of the extrapolation time to the averaging time.

It is clear from the above equations that errors can be reduced by increasing the cell volume, averaging time, or number of ensembles. While this also increases the computational cost, the savings relative to methods that do not use a multi-timescale algorithm

grows as the separation between continuum and molecular time scales increases. As explained in Section 2.2, the continuum time step scales with the characteristic time of flows on the grid size, $\rho \Delta x \Delta y / \mu$ for low Reynolds number flow. A longer macroscopic time scale allows both Δt_{FD} and N_{cell} to be increased. This in turn allows larger averaging times, and all of these changes reduce the noise. To illustrate the importance of time scale separation in the numerical accuracy, we test our method for two different grid sizes and macroscopic time scales.

3.1 Channel flow with small separation of time scales

To demonstrate our time scheme, we first simulate channel flow with a relatively small channel width $L_y = H = 109.5\sigma$. Periodic boundary conditions with period $L_x = 15.6\sigma$ and $L_z = 4.82\sigma$ are applied along x and z directions. As described in Section 2.1, the whole simulation domain is divided into two regions. For $y < 93.9\sigma$ MD simulation is used, and for $y > 46.9\sigma$ the continuum NS equations (2.2) are solved with a grid size of $\Delta x = \Delta y = 15.6\sigma$. The bottom wall is always kept stationary, and the flow is driven by moving the top wall in the x direction at velocity U_w. At $t=0$, the top wall starts moving, and the evolution is described by

$$U_w(t) = 2.5 \left[1 - \cos\left(2\pi t / t_p\right) \right] \sigma / \tau, \tag{3.3}$$

where $t_p = 1000\tau$ is the period of the wall motion and represents the time scale associated with macroscopic motion.

Since the characteristic time of flow on the grid scale is $\rho \Delta x \Delta y / \mu \sim 90\tau$, we choose the continuum time step as $\Delta t_{FD} = 10\tau$. MD simulations are performed over two shorter time intervals of $\Delta t_1 = \Delta t_2 = 0.5\tau$ before extrapolation. The microscopic state is then re-initialized over the relaxation time of $\Delta t_r = 1.0\tau$. Therefore, during each iteration, MD calculations are performed for a total time of only 2τ instead of 10τ.

The simulation results are presented in Fig. 3. We show only the MD domain results and each line represents the time evolution of the streamwise velocity at a different height. The bottom line represents the velocity at $y = \Delta y / 2$, and y increases by Δy for each successive line. For reference purposes, the original hybrid simulation where the MD is integrated over the entire Δ_{FD} [9] was performed in the same geometry and the results are shown by dashed lines in Fig. 3. Ten independent simulations ($N_{ensemble} = 10$) in the MD region were used to reduce statistical fluctuations.

Although time extrapolation gives larger fluctuations in the lower regions compared with the original hybrid results, the essential features of the macroscopic flow are captured. Furthermore, the results in the coupling region (top line) agree remarkably well with original hybrid results. From the arguments leading to (3.1) and (3.2) we expect the extrapolation to introduce errors of order $\Delta U(\Delta t_{AV}) \Delta t_{FD} / \Delta t_{AV} \sim 0.1\sigma / \tau$. This is comparable to the fluctuations found at the smallest y.

To estimate the fractional error, (3.1), we must divide the thermal fluctuations by the expected change in velocity, $\bar{U}_2 - \bar{U}_1$. Assuming that the velocity changes linearly with
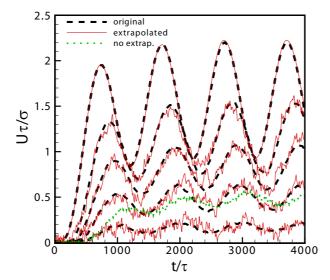
Figure 3: The time evolution of streamwise velocities in a relatively small simulation cell $H=109.5\sigma$. Velocities at grid centers within the MD domain are shown and higher velocities correspond to larger y. The dashed black lines represent results from the original hybrid method [9] and the thin red lines are the results with time extrapolation. The dotted green line shows the velocity at the second grid center for an algorithm that did not use extrapolation to reinitialize the MD simulations. All results were averaged over ten independent MD runs to reduce thermal fluctuations.

height y, $\bar{U}_2 - \bar{U}_1 \sim (y/H) 2\pi A/t_p$, and the fractional error from (3.1) is about 6.4. At first it is surprising that the method is stable when the signal is smaller than the noise. The reason is that the noise from different intervals and cells adds incoherently and there are many time steps per period. Thus the absolute errors remain bounded and the results follow the correct solution.

One might be tempted to skip the extrapolation step when the fractional error is greater than one. This does reduce the noise in the velocity, but it also introduces a significant time lag into the equations. To illustrate this we reran the simulation using the extrapolated boundary conditions from the continuum regime, but not constraining velocities in the remainder of the MD region during the relaxation time. The time dependence of the streamwise velocity in the second grid layer is shown as a dotted green line in Fig. 3. This curve lags the other results by about a quarter of the period and the mean value of the velocity is also depressed. There is a clear benefit to using the extrapolated velocities even though they increase noise.

3.2   Channel flow with large separation of time scales

In the second example, we simulate a system with twice the channel width $L_y = H = 218.9\sigma$. The dimensions in the x and z directions are $L_x = 31.3\sigma$ and $L_z = 4.28\sigma$. The larger width allows us to double the grid size $\Delta x = \Delta y = 31.3\sigma$. A much larger time step $\Delta t_{FD} = 50\tau$ and a correspondingly larger average time $\Delta t_1 = \Delta t_2 = 2.5\tau$ can then be used. The relaxation time after extrapolation is chosen as $\Delta t_r = 5.0\tau$ in this simulation.

As in the first example, the bottom wall is always kept stationary and the top wall moves sinusoidally with time according to

$$U_w(t) = 5.0 \left[1 - \cos\left(2\pi t / t_p \right) \right] \sigma / \tau. \tag{3.4}$$

The amplitude of oscillation is doubled so that the shear-rate in the simulations is the same and the period is increased in proportion to other times, $t_p = 5000\tau$.

The results are shown in Fig. 4. As before, the original hybrid simulation that integrates MD equations for all times is performed first as a reference and the results are displayed as dashed lines. Successively higher lines represent the time evolution of streamwise velocities at successively higher grid centers. Ten independent simulations in the MD region were used to reduce thermal fluctuations. As shown in Fig. 4, the agreement between extrapolated and original algorithms is much better than the first example with smaller grid size.
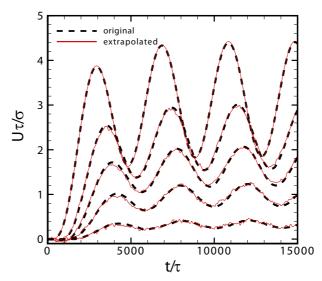

Figure 4: The time evolution of streamwise velocities in a larger simulation cell $H = 218.9\sigma$. Velocities at grid centers within the MD domain are shown and higher velocities correspond to larger y. The dashed black lines show results from the original hybrid method [9] and the thin red lines are the results with time extrapolation. All results were averaged over ten independent MD runs to reduce thermal fluctuations.

Increasing the grid size reduces thermal noise in our time scheme in two ways. First, the increasing separation between the continuum time step and MD time step allows us to average over longer times. Second, increasing the grid size also increases the number of particles N_{cell} in (3.2), and this also improves the signal to noise ratio. Since the ratio $\Delta t_{FD} / \Delta t_{AV}$ is the same as in the first example, the absolute error in the velocity decreases in proportion to the reduction in $\Delta U(\Delta t_{AV})$. The 4-fold increase in N_{cell} and 5-fold increase in Δt_{AV} reduce the estimate of the noise by $\sqrt{20}$ to $0.026\sigma/\tau$. As above, this is comparable to the fluctuations in the results for the smallest y. The estimated fractional error from (3.1) is reduced to 0.7. While this is still large, the effect on the results is reduced because of the incoherent addition of errors at different times and cells.

4   Conclusions

In this paper, we have implemented a multi-timescale algorithm to further improve the efficiency of the hybrid method developed in [9] for simulating dynamic micro/nano fluidics. In this scheme, molecular dynamics is adopted in small crucial regions and continuum hydrodynamics is employed in the remaining bulk regions. The coupling between these two descriptions is through "constrained dynamics". Our time approach is based on the observation that the continuum macro time step is typically orders of magnitude larger than molecular micro time step. This separation of time scales allows us to treat the molecular dynamics during each macro time step as in quasi-steady state. Therefore, during each iteration of the hybrid calculation, instead of performing the MD simulation in the entire macro time step, we perform MD calculations in two short time intervals and linearly extrapolate the macroscopic velocities over the macro time step. The particle velocities are then re-initialized based on the extrapolated macroscopic velocities to start the next iteration.

We demonstrated the implementation of our time scheme in hybrid simulations using examples of isothermal channel flow driven by sinusoidal wall motion. The results show that time extrapolation increases thermal fluctuations. However, the essential characteristics of macro motion can still be captured with reduced computational effort. Moreover, as shown in Figs. 3 and 4, comparison between results with small and large time separation reveals that the results converge to the correct solution with increasing time separation. Our results indicate that through combination of this time approach and hybrid "domain decomposition", both the temporal and spatial scales accessible to molecular simulations can be substantially extended without significantly increasing computational cost.

Acknowledgments

References

[1] S. T. O'Connell, and P. A. Thompson, Molecular dynamics-continuum hybrid computations: A tool for studying complex fluid flows, Phys. Rev. E 52 (1995) R5792-5795.
[2] N. G. Hadjiconstantinou and A. T. Patera, Molecular dynamics-continuum representation for dense fluid systems, Int. J. Modern Phys. C 8 (1997) 967-976.
[3] N. G. Hadjiconstantinou, Hybrid atomistic-continuum formulations and the moving contact-line problem, J. Comput. Phys. 154 (1999) 245-265.
[4] E. G. Flekkoy, G. Wagner and J. Feder, Hybrid model for combined particle and continuum dynamics, Europhys. Lett. 52 (2000) 271-276.

[5] G. Wagner, E. G. Flekkoy, J. Feder and T. Jossang, Coupling molecular dynamics and continuum dynamics, Comput. Phys. Commun. 147 (2002) 670-673.

[6] G. Wagner and E. G. Flekkoy, Hybrid computations with flux exchange, Phil. Trans. R. Soc. Lond. A 362 (2004) 1655-1665.

[7] R. Delgado-Buscalioni and P. V. Coveney, Continuum-particle hybrid coupling for mass, momentum and energy transfers in unsteady fluid flow, Phys. Rev. E 67 (2003) 046704-1-046704-13.

[8] R. Delgado-Buscalioni and P. V. Coveney, Hybrid molecular-continuum fluid dynamics, Phil. Trans. R. Soc. Lond. A 362 (2004) 1639-1654.

[9] X. B. Nie, S. Y. Chen, W. N. E and M. O. Robbins, A continuum and molecular dynamics hybrid method for micro- and nano-fluid flow, J. Fluid Mech. 500 (2004) 55-64.

[10] X. B. Nie, S. Y. Chen and M. O. Robbins, hybrid continuum-atomistic simulation of singular corner flow, Phys. Fluids 16 (2004) 3579-3591.

[11] X. B. Nie, M. O. Robbins and S. Y. Chen , Resolving singular forces in cavity flow: Multiscale modeling from atomic to millimeter scales, Phys. Rev. Lett. 96 (2006) 134501.

[12] J. Liu, S. Y. Chen, X. B. Nie and M. O. Robbins, A continuum-atomistic simulation of heat transfer in micro- and nano-flows, J. Comput. Phys. 227 (2007) 279-291.

[13] Y. Wang and G. He, A dynamic coupling model for hybrid atomistic-continuum computations, Chem. Eng. Sci. 62 (2007) 3574-3579.

[14] T. H. Yen, C. Y. Soong and P. Y. Tzeng, Hybrid molecular dynamics-continuum simulation for nano/mesoscale channel flows, Microfluid Nanofluid 3 (2007) 665-675.

[15] W. Ren and W. E, Heterogeneous multiscale method for modeling of complex fluids and micro-fluidics, J. Comput. Phys. 204 (2005) 1-26.

[16] W. E, B. Engquist, X. Li, W. Ren and E. Vanden-Eijnden, Heterogeneous multiscale methods: A review, Commun. Comput. Phys. 2 (2007) 367-450.

[17] I. G. Kevrekidis, C. W. Gear and G. Hummer, Equation-free: The computer-aided analysis of complex multiscale systems, AIChE J. 50 (2004) 1346-1355.

[18] G. S. Grest and K. Kremer, Molecular dynamics simulation for polymers in the presence of a heat bath, Phys. Rev. A 33 (1986) 3628-3631.

[19] R. Peyret and T. D. Taylor, Computational Methods for Fluid Flow, Springer (1983).